Brillouin and ultrasonic studies of phase transitions in Cs_2CdBr_4. I. Experimental

P. Kužel and P. Moch
Laboratoire des Propriétés Mécaniques et Thermodynamiques des Matériaux du Centre National de la Recherche Scientifique, Université Paris-Nord, Avenue J. B. Clément, 93430 Villetaneuse, France

A. Gomez-Cuevas
Departamento de Fisica de la Materia Condensada, Facultad de Ciencias, Universidad del Pais Vasco, Apartado 644, Bilbao, Spain

V. Dvořák
Institute of Physics, Na Slovance 2, 180 40 Prague 8, Czech Republic
(Received 12 July 1993)

The phase transitions in Cs_2CdBr_4 have been studied by means of Brillouin scattering and ultrasonic measurements. The sequence *Pnma* $\overset{252\text{ K}}{\leftrightarrow}$ incommensurate $\overset{235\text{ K}}{\leftrightarrow}$ $P2_1/n11$ gives rise to significant anomalies of both real and imaginary parts of the elastic constants. In the case of C_{44}, a strong asymmetric broadening of the Brillouin lines was observed in the IC phase and several degrees above the *Pnma* $\leftrightarrow$ IC transition. The differences between Brillouin and ultrasonic results concerning C_{22} and C_{44} suggest a strong frequency dependence of the process governing the above-mentioned sequence of phase transitions. A low-temperature transition at 156 K has been studied; it presents a considerable softening of shear stiffness constants. Selection rules for Brillouin scattering are greatly affected at the transitions to monoclinic and triclinic phases, allowing to measure the shear stiffness constants with a good accuracy. A detailed discussion of the phenomena linked to the monoclinicity is provided. In addition, the ultrasonic experiments have confirmed the existence of a previously reported phase transition at 208 K.

I. INTRODUCTION

Cs_2CdBr_4 is one of the β-K_2SO_4 family of crystals and, like most of them, it shows an incommensurate phase: together with Cs_2HgBr_4, it exhibits an interesting behavior since the lock-in phase transition occurs at the center of Brillouin zone. The space-group symmetry of this compound was found to be *Pnma* at room temperature.[1] Below that temperature, it undergoes several phase transitions. Five phase transitions have been reported up to now: at $T_i=252$,[2-7] $T_L=237$,[2-7] $T_{L'}=208$,[4,7] $T_C=156$,[2,3,5-7] and $T_{C'}=130$ K.[7] However, the observations reported in the literature agree with each other only in the sequence *Pnma*↔incommensurate↔commensurate (referred to as the "incommensurate sequence" in the following). The transition at 156 K was not observed by Maeda, Honda, and Yamada[4] (dielectric, x-ray measurements). The two remaining phase transitions, which apparently are not easily observable, have been detected only by Zaretskii and Depmeier[7] (both transitions; x-ray measurements) and by Maeda, Honda, and Yamada[4] (transition at 208 K only). In addition, the existence of these two new phase transitions reveals some contradictions concerning the symmetry of the low-temperature phases. A careful study of the bibliography shows the following picture:

T_i 252 K	T_L 237 K	$T_{L'}$ 208 K	T_C 156 K	$T_{C'}$ 130 K
I	II (IC)	III (C)	IV	
		III a / III b	IV a	IV b
[1] Pnma	[6] $P^{nma}_{\bar{1}ss}$ ($\mathbf{k}_o=\delta\mathbf{a}^*$)	[4] $P2_1/n11$	[8] $P\bar{1}$?	[5] $P\bar{1}$
		[5,6] $P2_1/n11$ or [4] $P\bar{1}$		
		2nd order	1st order	2nd order	2nd order	2nd order

($Z=4$ in all phases).

The incommensurate modulation appears along the **a** axis and the modulation wave vector exhibits a slight linear decrease with decreasing temperature, from $\delta \approx 0.2$ at T_i to $\delta \approx 0.15$ at T_L.[4] The modulation of the structure is characterized by a rotation of the $CdBr_4$ tetrahedra around **a** and by a slight translation of the caesium atoms along **b**.[6] The first-order phase transition at 237 K leading to the pseudoproper ferroelastic phase is interpreted as arising from a lock in at the Γ point. The existence of two distinct domain systems[4,5] explains the nearly orthorhombic symmetry of the x-ray diffraction patterns in this phase. A Raman study of Cs_2CdBr_4 was performed by Rodriguez *et al.*[8] An intense quasielastic scattering was observed near the incommensurate sequence; on the other hand, the spectra did not reveal any soft mode in this temperature range. The authors conclude that this sequence is governed by a dynamic order-disorder process, the static disorder being excluded by nuclear-quadrupole-resonance (NQR) measurements.[5] In contrast, the low-temperature transition III↔IV was found to be driven by a soft mode with B_{2g} symmetry; its temperature dependence is typical for a pseudoproper ferroelastic transition. The authors observe a breaking of the monoclinic selection rules just at this transition. This effect, which will be discussed below together with our Brillouin results, enables one to assume that the symmetry group of phase IVa is $P\bar{1}$. The optical birefringence method was used to determine the pressure-temperature phase diagram of the incommensurate sequence:[9] a triple point separating the paraelastic, ferroelastic, and incommensurate phases was found for a hydrostatic pressure of about 100 MPa. Above this critical pressure a direct second-order transition $Pnma \leftrightarrow P2_1/n11$ was observed. The elastic properties of Cs_2CdBr_4 were studied by means of ultrasonic-wave propagation.[8,10,11] The measurements concerned the incommensurate phase and a small temperature range above T_i and below T_L (all the diagonal stiffness constants were measured in the range of 230 to 270 K). Significant anomalies were measured for C_{44} and C_{22}. C_{44} shows a large hysteresis throughout the whole range of existence of the incommensurate phase.[11]

The present paper is mainly devoted to the experimental investigation of the elastic properties of Cs_2CdBr_4 near its phase transitions, derived from ultrasonic-propagation and Brillouin-scattering measurements. The results will be qualitatively compared with those expected from a static Landau model; the appropriate form of the corresponding free energy is introduced in Sec. II after a brief justification. Section III deals with experimental details. In Sec. IV we present and discuss the Brillouin spectra, while Sec. V is devoted to ultrasonic measurements. Throughout the paper we shall analyze the points of agreement and the discrepancies encountered when comparing the results to the predictions of the above-mentioned model, without going on to detailed calculations, which will be performed in the following paper (Paper II). Theoretical improvements including dynamics of the order parameter will be also presented in Paper II and compared to the experiments.

II. SCENARIO OF THE PHASE TRANSITIONS

As previously pointed out, the origin of the phase transitions (PT's) at T_i, T_L, and T_C seems rather well understood. The incommensurate (IC) phase is due (as in $NaNO_2$ for example) to the pseudo-Lifshitz invariant,[12] which couples two one-component modes p and q of $B_{3g}(yz)$ and $A_u(xyz)$ symmetry, respectively:

$$\frac{\sigma}{2}\left[\frac{dp}{dx}q - p\frac{dq}{dx}\right].$$

(We shall always use the system of coordinate axes x, y, z parallel to the orthorhombic crystallographic axes **a**, **b**, **c**.) Consequently, the harmonic part of the free energy F_k corresponding to these two modes propagating in the **k** $(k,0,0)$ direction reads:[13]

$$F_k = \frac{1}{2}\left[a_0 + \frac{a}{2}k^2\right]p_k p_k^* + \frac{1}{2}\left[b_0 + \frac{b}{2}k^2\right]q_k q_k^* + i\frac{\sigma k}{2}(p_k q_k^* - p_k^* q_k) \quad a,b>0, \quad b_0 > a_0 . \tag{1}$$

If the modes $p_{k=0}$ and $q_{k=0}$ are sufficiently close to each other and if the coupling between them is strong enough (more specifically if[12] $2\sigma^2/a > b_0 - a_0$), a minimum can occur near the Γ point on the lower-frequency mixed branch. This branch will hereafter be denoted $Q_1(k)$. Therefore the free-energy density describing the PT into the IC phase can be written in the usual form:

$$F_{Q_1} = \frac{1}{2}a_1(T-T_1)Q_1^2 + \frac{1}{4}B_1Q_1^4 + \cdots + \frac{1}{2}C_x\left[\frac{dQ_1}{dx}\right]^2 + \frac{1}{2}D_x\left[\frac{d^2Q_1}{dx^2}\right]^2 \quad C_x<0, \quad D_x>0 . \tag{2}$$

[This simple description leads to $k_0 = -C_x/2D_x$ for the incommensurate wave vector $\mathbf{k}_0$ $(k_0,0,0)$.]

Our experimental data (see Fig. 5) clearly suggest that the PT at T_C is driven by a Γ mode Q_2 of B_{1g} (xy) symmetry. The corresponding part of the free energy has obviously the form:

$$F_{Q_2} = \tfrac{1}{2}a_2(T-T_2)Q_2^2 + \tfrac{1}{4}B_2Q_2^4 + \cdots . \tag{3}$$

Before discussing the origin of the PT's at $T_{L'}$ and $T_{C'}$, let us look for a simple argument explaining the simultaneous existence of two (at least) different low-frequency modes. Very recently,[14] such an argument has been provided starting with the hexagonal prototype phase $P6_3/mmc$ which is common for the materials of the A_2BX_4 type. From compatibility relations it follows that an E_{2u} mode splits in the direction [001] into Σ_2 and Σ_4

branches; at the end of the Brillouin zone these branches acquire M_2 and M_4 symmetry, respectively [the point M is at $(0,0,c^*)$ where $\mathbf{c}$ is a lattice parameter in the orthorhombic phase—see Ref. 15 for the relations between orthorhombic and hexagonal unit cells]. It can be shown[14] that these branches may consist of librational modes of rigid $CdBr_4$ tetrahedra, which are the lowest-frequency external modes in Cs_2CdBr_4. Let us denote the triply degenerate M_4 modes at the M point as q_1,q_2,q_3. The mode q_1 is responsible for the virtual PT $P6_3/mmc(Z=2)\rightarrow Pnma\,(Z=4)$[15] and becomes a Γ mode of A_g (x^2,y^2,z^2) symmetry in the orthorhombic phase while the M_2 mode transforms into a B_{3g} mode $(p_{k=0})$. Thus, assuming that the doubly degenerate E_{2u} mode softens, one can explain the existence of two modes, i.e., M_4 and B_{3g} modes, on an equal footing as needed for the PT's into the orthorhombic and monoclinic phases. We shall pursue this idea even further by noting that there is also a low-frequency A_u mode $(q_{k=0})$ needed for explaining the IC phase since, in the orthorhombic phase, E_{2u} modes split into A_u and B_{3u} (x) modes. The assumed course of the dispersion branches relevant to the PT's is schematically plotted in Fig. 1 (branches which are not coupled to relevant ones are omitted for simplicity). It should be remembered that the branches should coalesce in pairs with nonzero slopes at the points $\frac{1}{2}\mathbf{a}^*$ and $\frac{1}{2}\mathbf{c}^*$ (Lifshitz invariants exist there). To meet this condition we need a low-frequency mode B_{1g} (xy)—later responsible for the PT at T_C—which combines at $\frac{1}{2}\mathbf{a}^*$ with the A_u mode via the branches Σ_4 and Σ_2 (see Fig. 1). There are no direct experimental evidences so far confirming this speculative scheme of dispersion branches in Cs_2CdBr_4.

We return now to the problem of what might be the origin of the PT's at $T_{L'}$ and $T_{C'}$. Let us first assume that these PT's are equitranslational. Obviously, the possible order parameters cannot belong to odd representations of *Pnma* since a loss of the inversion center has never been observed in Cs_2CdBr_4. Even representations B_{1g} and B_{2g} would induce pronounced anomalies of the elastic constants C_{66} and C_{55}, respectively, which have been observed neither near $T_{L'}$ nor near $T_{C'}$. Therefore we are left with the totally symmetric representation A_g, which would induce an isomorphous first-order PT. Experimental results[4,7] suggest, however, that these PT's are rather continuous than discontinuous. Nonequitranslational PT's are more probable, simply because they have already been observed in the isomorphous materials Rb_2ZnCl_4 and Cs_2HgBr_4.[5] It has been proved by neutron inelastic scattering[16] that the low-temperature PT from the lock-in improper ferroelectric phase both in Rb_2ZnCl_4 and in K_2ZnCl_4 is driven by the remaining soft modes corresponding to the three-dimensional representation M_4 of the hexagonal prototype phase. These soft modes q_2,q_3 remain degenerate in the ferroelectric phase and produce a doubling of the unit cell. By analogy we believe, as do the authors of Ref. 14, that these modes play some role in Cs_2CdBr_4, too. First we note that, unlike the situation in the ferroelectric phase (Rb_2ZnCl_4, K_2ZnCl_4), the degeneracy of q_2 and q_3 modes is lifted in the ferroelastic lock-in phase $P2_1/n11$ (Cs_2CdBr_4) due to the coupling term $m\varepsilon_4^s(q_2^2-q_3^2)$, where the index s denotes the spontaneous shear in the monoclinic phase. Obviously, this term contributes to the softening of the q_2 or q_3 mode depending on the sign of m. Now it is easy to show that freezing of a q_i mode would lead to a unit-cell doubling $(Z=8)$ only, but that the symmetry would remain monoclinic $P2_1/n11$. Consequently, there is no coupling like $q_i^n\varepsilon_j$ $(n=1,2,\ldots;\ j=5,6;\ i=2,3)$ and hence no pronounced anomalies in C_{jj} could be expected near a PT induced by q_i. Therefore the q_2 mode, for example, could be a candidate for the PT at $T_{L'}$ around which a small anomaly in C_{22} only has been observed (see Fig. 11). Unfortunately, however, we need to explain two PT's, at $T_{L'}$ and $T_{C'}$. It would seem quite natural to assume that the PT at $T_{C'}$ is driven by the q_3 mode, but this would destroy the center of inversion, which apparently does not occur. This fact leads us to the conclusion that the PT's at $T_{L'}$ and $T_{C'}$ might be in fact transitions into an IC phase followed by a corresponding lock-in PT due to a soft mode $q_{2,k}$ near the M point of the hexagonal prototype phase (the T point in the orthorhombic phase) at $\mathbf{k}=\mu\mathbf{b}^*+\frac{1}{2}\mathbf{c}^*$ $(\mu\cong\frac{1}{2})$, as was observed in K_2ZnCl_4.[16] The small elastic anomalies (see below) and the lack of change in the Raman spectra[8,14] below $T_{L'}$ are not contradictory to this hypothesis. On the other hand it should be pointed out that the PT's at $T_{L'}$ and $T_{C'}$ have not been seen in sensitive NQR measurements.[2] It might be possible that the existence of these two PT's depends on the sample preparation. Our hypothesis based exclusively on an analogy with the isomorphous K_2ZnCl_4 seems to be the most simply way to explain the extra PT's observed by some authors (including us—see below) in Cs_2CdBr_4. In between $T_{L'}$ and $T_{C'}$ there is the PT at T_C driven by the soft B_{1g} mode which reduces the symmetry to $P\bar{1}$. We propose to identify this soft mode with one observed in the (xy) Raman spectrum.[14] Note that this mode is also observed in other spectra according to the symmetry requirements for the selection rules[8,14] [(xz) in the monoclinic phase, any geometry in the triclinic one below T_C]. In conclusion, if our hypothesis is correct,

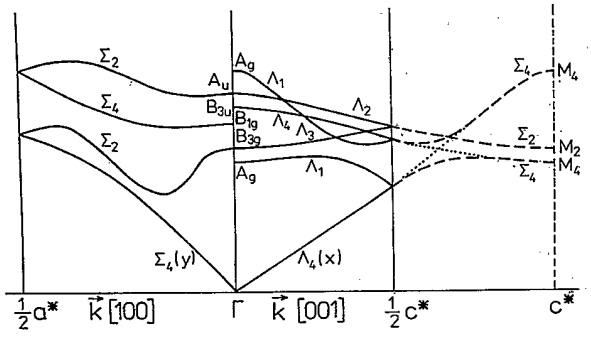

FIG. 1. Schematic picture of dispersion branches in the [100] and [001] directions of the Brillouin zone in the orthorhombic phase. The dashed lines correspond to the hexagonal phase. Remember that in the hexagonal phase the A_u and B_{3u} modes degenerate into an E_u mode.

the sequence of low-temperature phases in Cs_2CdBr_4 would be:

$$P2_1/n11(Z=4) \xrightarrow{T_{L'}} \text{IC} \xrightarrow{T_C} P\bar{1}(Z=4) \xrightarrow{T_{C'}} P\bar{1}(Z=8) .$$

Since, from the analysis of most experimental data, the transitions at $T_{L'}$ and at $T_{C'}$ only weakly affect the structural arrangement and the physical properties of Cs_2CdBr_4, and, more specifically, induce only small anomalies in its elastic constants, we shall use, in order to guide our interpretation, the previously proposed free-energy density:[8]

$$F=F_{Q_1}+F_{Q_2}+F_\varepsilon+F_{Q,\varepsilon} , \tag{4}$$

where F_ε is the elastic energy

$$F_\varepsilon=\frac{1}{2}\sum_{i,j=1}^{3} C_{ij}^0\varepsilon_i\varepsilon_j+\frac{1}{2}\sum_{i=4}^{6} C_{ii}^0\varepsilon_i^2 \tag{5}$$

and where $F_{Q,\varepsilon}$ describes the coupling of the order parameters to the strains and is written as

$$F_{Q,\varepsilon}=\sum_{i=1}^{3}(F_iQ_1^2+H_iQ_2^2)\varepsilon_i+fQ_1\varepsilon_4+gQ_1Q_2\varepsilon_5+hQ_2\varepsilon_6 . \tag{6}$$

Notice that the symmetry of Q_2 is B_{1g} (xy) rather than B_{2g} (xz), and therefore the roles of ε_6 and ε_5 are interchanged with respect to the original paper.[8] Indeed, the chosen form (6) can only describe the incommensurate sequence followed by the III↔IV transition at T_C. Neglecting dynamics and fluctuations, one easily calculates the anomalies of the elastic constants deriving from this model. The most pronounced features are believed to arise from the bilinear terms $(fQ_1\varepsilon_4, gQ_1Q_2\varepsilon_5, hQ_2\varepsilon_6)$, which deeply affect the transverse constants (C_{44}, C_{55}, C_{66}). From the analysis of our experimental data, it will be shown that improvements of this model including dynamics have to be performed. This will be the aim of Paper II.

III. EXPERIMENTAL DETAILS

Crystals of Cs_2CdBr_4 were grown from the melt by the Bridgman method. They show a good optical quality and they easily cleave perpendicularly to the c axis. They were oriented with the aid of optical methods and conveniently cut. The refractive indices were measured at room temperature: $n_a=1.699, n_b=1.683, n_c=1.675$.

The Brillouin experiments were performed using a five-pass Fabry-Pérot interferometer which was described previously.[17] The finesse of the instrument is about 50 for the free spectral ranges used (between 10 and 30 GHz). Thus, in backscattering experiments, where the results are not influenced by geometrical broadening, the full width at half maximum (FWHM) of a Brillouin line can be reasonably evaluated if it exceeds about 150 MHz. The 5145-Å line of an argon single-mode laser was used. The incident radiation power was taken as small as possible in order to avoid sample heating: it varied from a few tens of mW for scattering by longitudinal modes up to 300 mW when studying transverse modes, which have a very weak intensity.

Ultrasonic measurements were made using two different types of MATEC ultrasonic equipment. Absolute sound velocities were determined by the pulse-echo overlap method with a MATEC 6600 pulse generator. The accuracy of the absolute values of the velocity can reach 0.1%: however, there are often ambiguities concerning the proper choice of the overlapping peaks; since, throughout the study, we only focused on the temperature variations of the elastic constants, we did not attempt to derive absolute values completely consistent with the other experimental data (previously published ultrasonic measurements[8,10] and our own Brillouin results). This explains some small differences far from the PT, between ultrasonic and Brillouin values appearing in the rest of this paper. Measurements of the temperature dependence of the ultrasonic-pulse transit time and of its attenuation were performed using a computerized coherent phase system detecting transit-time changes down to 1 part in 10^5. The rate of temperature change was about 0.05 K/min in the vicinity of the transition temperatures and 0.1 K/min in the other temperature regions. Coaxially gold-plated X- or Y-cut quartz transducers of fundamental frequency 10 MHz were used to generate longitudinal and shear modes, respectively, along the crystallographic directions. The transducers were bonded to the crystal with bis-(2-ethylhexyl)-sebacate.

IV. BRILLOUIN SCATTERING

All the elastic stiffnesses were calculated using the room-temperature values of the refractive indices and of the crystallographic data (to calculate the density), ignoring their temperature dependence. The values of all the orthorhombic elastic constants measured at room temperature are reported in Table I.

In Brillouin scattering we have observed three phase transitions: I↔II at 252 K, II↔III at 235 K, and III↔IV at 156 K. Therefore the discussion of the Brillouin results will concern mainly these three transitions. Notice that the temperature of the transition II↔III differs by 2 K from the data previously published (237 K), but agrees with our ultrasonic results (see below).

In order to present the experimental results clearly, we introduce the following notation: the elastic constant related to the acoustic phonons propagating in the direction **e** along one of the orthorhombic axes is written as $\gamma_j(\mathbf{e})$ [with $\gamma_j(\mathbf{e})=C_{jj}$ $(j=1,\ldots,6)$ in the orthorhombic phase, e.g., $\gamma_4(\mathbf{b})=\gamma_4(\mathbf{c})=C_{44}$ in the orthorhombic phase]. For the longitudinal or quasilongitudinal modes, the axis along which the phonons propagate is unambiguously determined by the index j, so we can abbreviate: $\gamma_j(\mathbf{e})=\gamma_j$ for $j=1,2,3$ (e.g., $\gamma_2=C_{22}$ in the orthorhombic phase).

A. Backscattering

The two lower transitions (235, 156 K) are clearly marked in the low-symmetry phases by the occurrence of

TABLE I. Values of elastic constants at 295 K. The experimental error for all the values is ∓ 0.1 GPa.

Elastic constants	(GPa)
C_{11}	22.0
C_{22}	14.6
C_{33}	14.7
C_{12}	7.6
C_{13}	7.7
C_{23}	6.6
C_{44}	2.85
C_{55}	4.15
C_{66}	3.25

new spectral lines which are forbidden in the backscattering arrangement[18] above the transition temperatures. The observed selection rules in phase(s) III correspond to the monoclinic spatial groups and the selection rules of phase(s) IV correspond to the triclinic ones.

First, we analyze the monoclinicity effects observed in the backscattering spectra below 235 K. Let us suppose that the incident beam is polarized along one of the orthorhombic axes and propagates along another one. The only allowed Brillouin lines in the orthorhombic phase are related to the longitudinal modes and give access through their velocities to the "longitudinal" elastic constants C_{11}, C_{22}, or C_{33}. They are observed with incident and scattered polarizations parallel to each other. In the monoclinic phase, for light propagating along the **a** axis, the two transverse modes remain forbidden, but the longitudinal mode related to C_{11} is also observed in crossed polarizations along **b** and **c**. For propagation along the **b** (or **c**) axis there exists only one purely transverse mode, C_{66} (or C_{55}), which is allowed when the incident and scattered beams are polarized perpendicularly to each other. The two remaining modes—quasilongitudinal and quasitransverse—are related to γ_2 (or γ_3) and $\gamma_4(\mathbf{b})$ [or $\gamma_4(\mathbf{c})$], respectively, and are allowed with parallel polarizations. The expressions for these elastic constants are approximately given by

$$\gamma_2 \cong C_{22} + \frac{C_{42}^2}{C_{22}-C_{44}}, \quad \gamma_4(\mathbf{b}) \cong C_{44} - \frac{C_{42}^2}{C_{22}-C_{44}} \tag{7a}$$

for propagation along **b**; and by

$$\gamma_3 \cong C_{33} + \frac{C_{43}^2}{C_{33}-C_{44}}, \quad \gamma_4(\mathbf{c}) \cong C_{44} - \frac{C_{43}^2}{C_{33}-C_{44}} \tag{7b}$$

for propagation along **c**. In the above expressions, we neglected all the higher-order terms in morphic elastic constants: $[4C_{4i}/(C_{ii}-C_{44})]^2 \ll 1$; $i=2,3$.

Figure 2 shows the measured relative intensities of the lines between T_L and T_C. We have to mention that all the predicted lines are observed; the ratios r_{42}^a and r_{43}^a

TABLE II. Calculated approximate relative values of the intensities of Brillouin lines for backscattering in the monoclinic phase. $I_i^{\alpha\beta}(\mathbf{e})$ stands for the intensity originating in the scattering on an acoustic phonon, related to the elastic constant γ_i, which propagates in the direction **e**; the polarizations of the incident and of the scattered beam are α and β, respectively. $\Delta n_{c'b'}$ is the difference between the principal values of the refractive indices in the (bc) plane for the monoclinic phase; the axes of the indicatrix do not coincide with the crystallographic ones.

	Term I	Term II	Term III
$\left[\frac{I_2^{aa}(\mathbf{b})}{I_2^{cc}(\mathbf{b})}=\frac{p_{12}^2}{p_{32}^2}\right]$			
$r_{42}^c=\frac{I_4^{cc}(\mathbf{b})}{I_2^{cc}(\mathbf{b})}=\frac{\gamma_2}{\gamma_4(\mathbf{b})}$	$\left[-\frac{C_{42}}{C_{22}-C_{44}}\right.$	$+\frac{p_{34}}{P_{32}}$	$\left.+\frac{\sin 2\theta}{p_{32}}\left[\frac{1}{n^2}-2p_{44}\right]\frac{\Delta n_{c'b'}}{n}\right]^2$
$r_{42}^a=\frac{I_4^{aa}(\mathbf{b})}{I_2^{aa}(\mathbf{b})}=\frac{\gamma_2}{\gamma_4(\mathbf{b})}$	$\left[-\frac{C_{42}}{C_{22}-C_{44}}\right.$	$+\frac{p_{14}}{p_{12}}$	$\left.+0\right]^2$
$r_{62}=\frac{I_6^{ac}(\mathbf{b})}{I_2^{cc}(\mathbf{b})}=\frac{\gamma_2}{C_{66}}$	$\left[0\right.$	$+\frac{p_{56}}{p_{32}}$	$\left.+\frac{1}{2}\frac{\sin 2\theta}{p_{32}}\left[\frac{1}{n^2}-2p_{66}\right]\frac{\Delta n_{c'b'}}{n}\right]^2$
$\left[\frac{I_3^{aa}(\mathbf{c})}{I_3^{bb}(\mathbf{c})}=\frac{p_{13}^2}{p_{23}^2}\right]$			
$r_{43}^b=\frac{I_4^{bb}(\mathbf{c})}{I_3^{bb}(\mathbf{c})}=\frac{\gamma_3}{\gamma_4(\mathbf{c})}$	$\left[-\frac{C_{43}}{C_{33}-C_{44}}\right.$	$+\frac{p_{24}}{p_{23}}$	$\left.+\frac{\sin 2\theta}{p_{23}}\left[\frac{1}{n^2}-2p_{44}\right]\frac{\Delta n_{c'b'}}{n}\right]^2$
$r_{43}^a=\frac{I_4^{aa}(\mathbf{c})}{I_3^{aa}(\mathbf{c})}=\frac{\gamma_3}{\gamma_4(\mathbf{c})}$	$\left[-\frac{C_{43}}{C_{33}-C_{44}}\right.$	$+\frac{p_{14}}{p_{13}}$	$\left.+0\right]^2$
$r_{53}=\frac{I_5^{ab}(\mathbf{c})}{I_3^{bb}(\mathbf{c})}=\frac{\gamma_3}{C_{55}}$	$\left[0\right.$	$+\frac{p_{65}}{p_{23}}$	$\left.+\frac{1}{2}\frac{\sin 2\theta}{p_{23}}\left[\frac{1}{n^2}-2p_{55}\right]\frac{\Delta n_{c'b'}}{n}\right]^2$

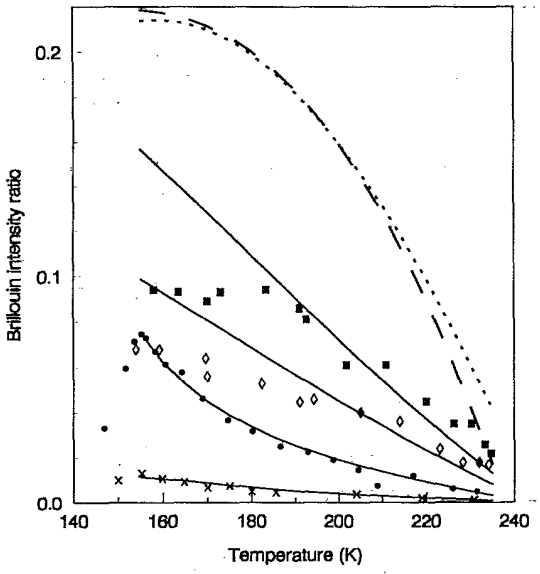

FIG. 2. Measured intensity ratios of the Brillouin lines in the monoclinic phase: $\blacksquare r^c_{42}, \Diamond r^b_{43}, \bullet r_{62}, \times r_{53}$ (see Table II for the significance of r^a_{ij}); r^a_{42} and r^a_{43} are smaller than 1%. Dotted and dashed line: contributions of C_{42} and C_{43} (calculated from γ_3—see text) to r^c_{42}, r^a_{42} and r^b_{43}, r^a_{43}, respectively. Solid lines: fits neglecting terms other than II (see Table II). The variation versus temperature of the squares of the morphic photoelastic constants is supposed to be linear.

(notation defined in Table II) are smaller than 1% and the intensities $I^{aa}_4(\mathbf{b})$ and $I^{aa}_4(\mathbf{c})$ are comparable with the background and therefore cannot be studied quantitatively. The calculated relative intensities of the allowed modes in the monoclinic phase are presented in Table II. Three terms appear in the expressions for the intensities of the transverse and of the quasitransverse modes. The first one (term I) is due to the obliquity of the mode polarization (related to the nonzero values of C_{42} and C_{43}, which vanish in the orthorhombic phase). The second (term II) is due to the presence of morphic photoelastic coefficients and the last term (term III) comes from the rotation θ of the optical indicatrix. In order to simplify the expressions we took into account only the first-order terms[21] in morphic elastic and photoelastic constants and in the refractive-index difference $\Delta n_{c'b'}$. In addition, in Cs_2CdBr_4 one can neglect term III: the intensity ratio related to the second (static) part of term III is smaller than 0.005% ($|\Delta n_{c'b'}|/n \lesssim 0.01, |p_{44}| \lesssim 0.06|p_{32}|, \ldots,$); in order to evaluate the first (dynamic)[19] part of term III, it is necessary to know the absolute values of p_{32} and of p_{23}. Our experiments show that the intensities of longitudinal modes in Cs_2CdBr_4 are of the same order of magnitude as those observed in quartz. The photoelastic constants of quartz are known:[20] $p_{12} \cong p_{13} \cong p_{31} \cong 0.25$. Taking into account the compared values of the elastic constants in quartz and in Cs_2CdBr_4, the contribution of term III to the intensity ratio is evaluated to be 0.1% at most and cannot explain the measured ratios which reach several percent. Term I is linked to the obliquity correction of the γ_i constants (7a) and (7b); therefore we will discuss the relative contributions of terms I and II after the presentation of all the backscattering results.

We did not observe any change in the selection rules at 208 K. On the contrary, our measurements show that the structure becomes triclinic below 156 K: we have observed several quasitransverse Brillouin lines which are forbidden in the monoclinic phase. Unfortunately, a quantitative analysis of the intensities in the triclinic phase is not very fruitful because all the acoustic phonons become allowed as a rule: their intensities depend on many morphic constants which in practice cannot be unambiguously determined. Therefore we do not give any analysis of the line intensities below 156 K.

The γ_1 constant (C_{11} in the orthorhombic and in the monoclinic phase) presents only very small anomalies (Fig. 3). On the other hand, for propagation along **a** with incident and scattered beams perpendicularly polarized—geometry $x(yz)\bar{x}$—an intense quasielastic scattering progressively appears in the Brillouin spectrum at about 20 K above the PT into the IC phase and reaches its maximum near T_i. Its intensity slowly decreases between T_i and T_L and abruptly disappears at T_L (Fig. 4). The existence of a central peak in the $x(yz)y$ Raman spectrum has already been reported by Rodriguez *et al.*[8] We attribute the quasielastic Brillouin feature to this central peak which is related to an overdamped mode (librations of $CdBr_4$ tetrahedra) of B_{3g} (yz) symmetry; in Paper II we shall prove that this overdamped mode behaves in practice as a pure relaxator, softening when approaching the PT into the IC phase. This hypothesis is also supported by our results for 90° scattering (see below).

In Fig. 5 the results of backscattering along the **b** orthorhombic axis are presented. The anomalies observed at T_C are typical for a pseudoproper ferroelastic second-order phase transition governed by a soft mode at the Γ point with B_{1g} (xy) symmetry. The softening of $\gamma_6(\mathbf{b})$ is then explained by the bilinear coupling between the shear strain ε_6 and the order parameter Q_2 ($[hQ_2\varepsilon_6$, see Eq. (6)]. The constant γ_2 reveals two jumps (at T_C and T_L) prob-

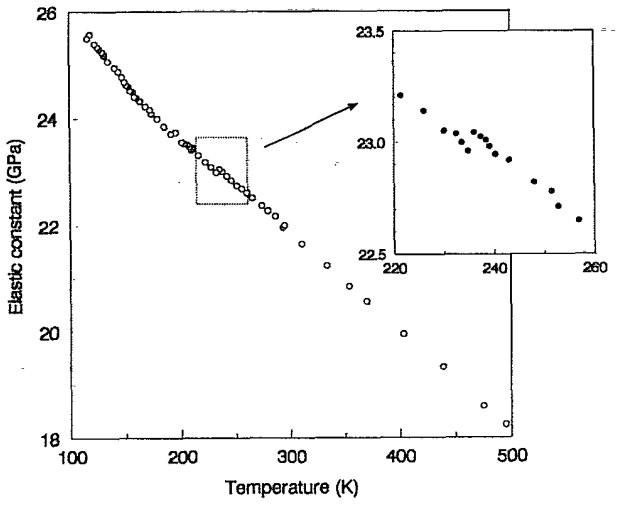

FIG. 3. Temperature dependence of γ_1 (C_{11} in the orthorhombic and in the monoclinic phase) measured in backscattering along the **a** orthorhombic axis.

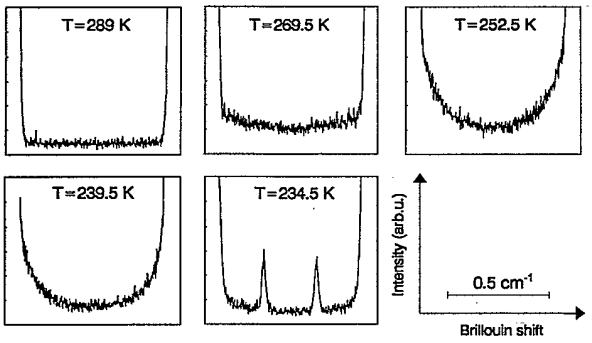

FIG. 4. Evolution of the $x(yz)\bar{x}$ spectra with temperature. Both vertical and horizontal scales are the same in all figures.

ably related to linear-quadratic couplings ($F_2Q_1^2\varepsilon_2$ and $H_2Q_2^2\varepsilon_2$). The behavior of γ_2 is presented with an expanded temperature scale in Fig. 6 in order to show the incommensurate sequence with more detail. Notice that, instead of a jump at T_i, which would be expected (see Paper II), we observe a progressive softening beginning already at 320 K (softening of the elastic constant with respect to the regular linear behavior far above this temperature). The abrupt jump (0.2 K) at T_L is accompanied by a broadening of the spectral line. This broadening is slightly asymmetric as shown in Fig. 7.

The results of backscattering along the **c** axis are shown in Fig. 8. The behaviors of γ_3 and $\gamma_5(\mathbf{c})$ near T_C agree with the coupling to the B_{1g} soft mode (we give a more detailed discussion in Paper II).

Let us return to the monoclinicity effects. The temperature variation of γ_3 suffers an increase of slope at T_L, while both $\gamma_4(\mathbf{b})$ and $\gamma_4(\mathbf{c})$ decrease in the monoclinic phase, when the temperature is lowered. Notice that the obliquity contribution [(7a) and (7b)] to γ_3 is always positive and that the contributions to $\gamma_4(\mathbf{b})$ and $\gamma_4(\mathbf{c})$ are always negative. If we suppose that the increase of γ_3 in phase III with regard to its linear evolution in phase I is only due to the obliquity, we can calculate the variations of C_{22}, C_{44}, C_{42}, and C_{43} in this phase. At first sight the results are satisfactory: below T_L, one finds that the slope of the variation of C_{44} versus temperature is negative [while for $\gamma_4(\mathbf{b})$ and $\gamma_4(\mathbf{c})$ the slopes are positive—an analogous situation is found[21] for example in $RbLiSO_4$] as expected for a bilinear coupling of the shear

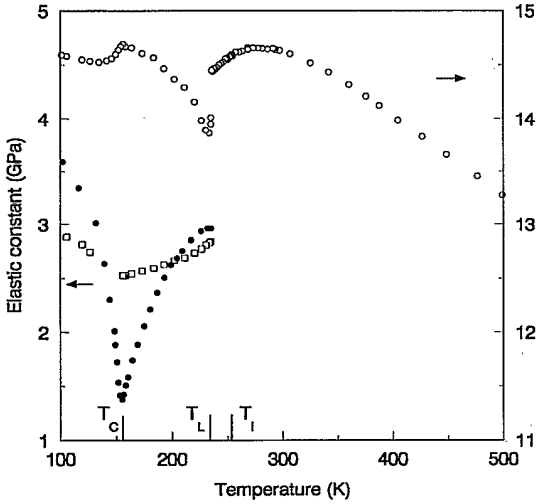

FIG. 5. Temperature dependence of γ_2 (C_{22} in the orthorhombic phase) (○), $\gamma_4(\mathbf{b})$ (□), and $\gamma_6(\mathbf{b})$ (C_{66} in the monoclinic phase) (●), measured in backscattering along the **b** orthorhombic axis.

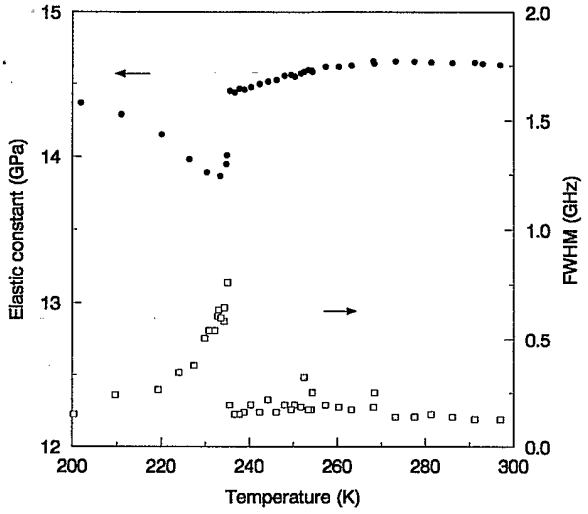

FIG. 6. Temperature dependence of γ_2(●) and of the FWHM of the related line (□) near the incommensurate sequence. Backscattering along the **b** orthorhombic axis.

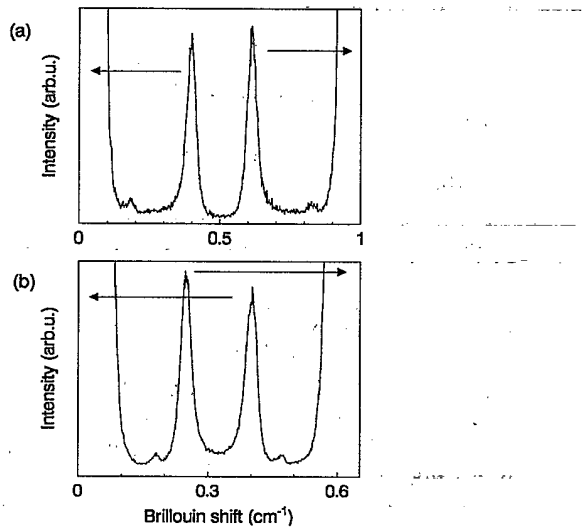

FIG. 7. Spectra obtained by backscattering along the **b** orthorhombic axis (the polarizations of both incident and scattered beams are parallel to the **c** orthorhombic axis) at 234.5 K just below the lock-in PT. Brillouin frequency ≈ 0.40 cm^{-1}. (a) Uncrossed Brillouin lines (free spectral range 1.0 cm^{-1}); (b) crossed Brillouin lines (free spectral range 0.65 cm^{-1}). The shape of the inelastic signal suggests a slightly asymmetric broadening of lines below T_L.

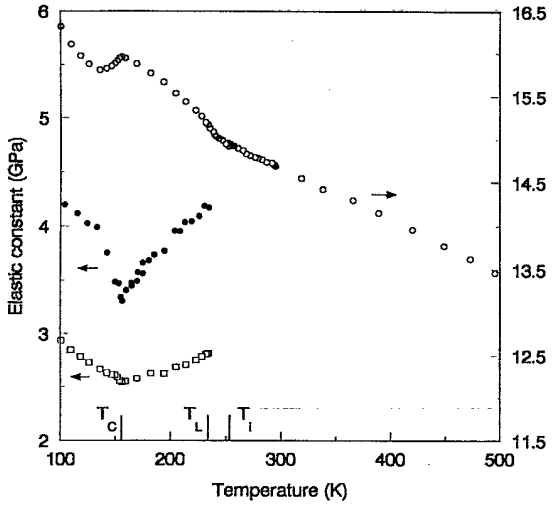

FIG. 8. Temperature dependence of γ_3 (C_{33} in the orthorhombic phase) (○), $\gamma_4(\mathbf{c})$ (□), and $\gamma_5(\mathbf{c})$ (C_{55} in the monoclinic phase) (●), measured in backscattering along the c orthorhombic axis.

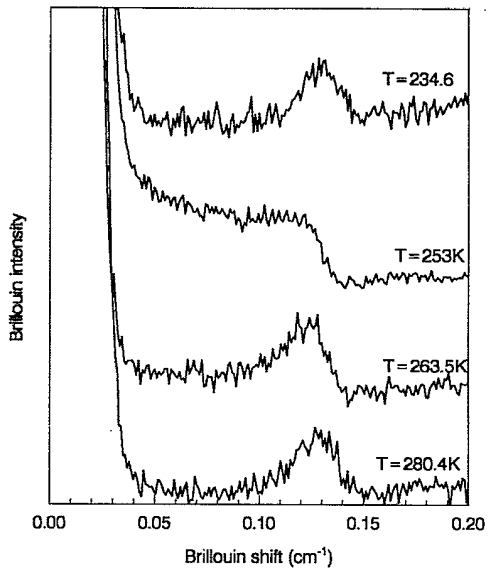

FIG. 9. Spectra measured in 90° scattering geometry at different temperatures around the incommensurate sequence. The scattering is related to $\gamma_4(\mathbf{b})$.

strain ε_4 to the order parameter ($fQ_1\varepsilon_4$). On the other hand, one can calculate the intensity ratios labeled in Table II using the derived values of the elastic constants and assuming that the contributions of the morphic photoelastic constants (term II in Table II) are negligible. The results are shown in Fig. 2 by the dotted and dashed curves for r^c_{42}, r^a_{42} and for r^b_{43}, r^a_{43}, respectively (indeed, r_{62} and r_{53} vanish in this approximation): they overestimate the experimentally observed ratios r^c_{42} and r^b_{43}. Consequently, the morphic photoelastic constants significantly contribute to these ratios, and/or the anomalies observed in γ_3 do not only derive from the occurrence of the morphic elastic constants: in this last case, C_{42} and C_{43} would have to be reevaluated. The morphic photoelastic constants are easily shown to be proportional to the order parameter Q_1 between T_L and T_C: the variation of the ratios p_{65}/p_{23} and p_{56}/p_{32} can be fitted directly from our experimental data concerning r_{62} and r_{53} (as shown above, r_{62} and r_{53} are given by term II only); this fit yields the variation of the order parameter: a critical exponent around 0.5 (value expected using a Landau model) gives a very good fit (Fig. 2). The calculated contributions of term II to r^c_{42}, r^a_{42}, r^b_{43}, and r^a_{43} in order to fit experimental data using the above evaluated C_{42} and C_{43} would lead to contradictions and unphysical results. In contrast, if one neglects term I, a reasonably good fit is obtained with morphic photoelastic constants following the above-mentioned variation of Q_1. To summarize, the oblicity calculated from the γ_3 temperature behavior looks to be significantly overestimated: $|C_{42}|$ and $|C_{43}|$ have to be reduced. Consequently their temperature variation cannot be determined from γ_3 and stays unknown. A simultaneous fit of elastic and photoelastic effects could indeed be performed, but, due to experimental uncertainties, it would be very imprecise. In our opinion one can conclude only that term I is smaller than term II.

B. 90° scattering

$\gamma_4(\mathbf{b})$ was studied by means of 90° scattering near the incommensurate sequence. The measured spectra are given in Fig. 9. The corresponding spectral line, which is well defined at room temperature, progressively broadens on its low-frequency side when approaching the IC phase. Several degrees above T_i the scattering profile becomes completely asymmetric and the maximum disappears. At the lock-in PT a well-defined line is suddenly restored. When the line is reasonably sharp the effective elastic constant $\gamma_4(\mathbf{b})$ is simply related to the frequency of this maximum: in Fig. 10 we have reported the corresponding temperature variation, derived from the shift of the

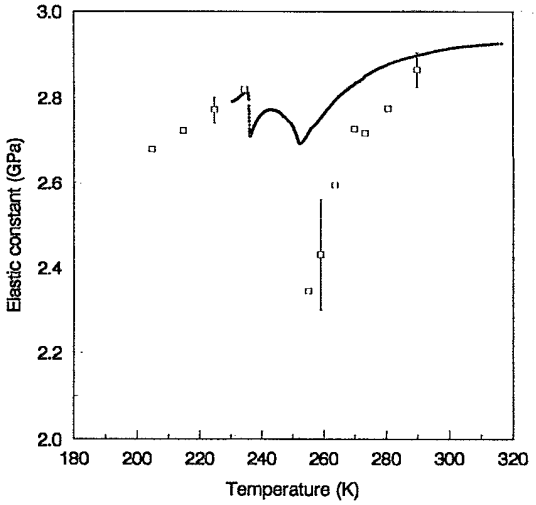

FIG. 10. Temperature dependence of $\gamma_4(\mathbf{b})$: (□) Brillouin scattering, (●) ultrasonic-wave propagation (heating).

maximum when it exists; but one has to keep in mind that for large broadening, i.e., for $T-T_i \lesssim 10$ K, this calculated value progressively loses its physical significance and it becomes questionable to define an elastic constant in this way. An attempt to analyze the corresponding shape in terms of an overdamped Lorentzian profile properly convoluted with the instrumental function (which can significantly shift the maximum in the case of strong asymmetry) often allows the derivation of a characteristic frequency and a damping constant; however, for the observed spectra, it is not possible to obtain a satisfactory fit. The measured spectra, which are related to the Fourier transforms of the appropriate correlation functions, among which appears the autocorrelation function of the shear strain ε_4, will be interpreted in Paper II as resulting from dynamic effects arising through the bilinear coupling between ε_4 and an overdamped soft mode.

V. ULTRASONIC MEASUREMENTS

The elastic stiffnesses were also calculated from ultrasonic experiments using sample lengths not corrected from thermal expansion. We have observed four phase transitions by means of ultrasound: at 252, at 235, at 208, and at 156 K. The behavior of γ_2 is shown in Fig. 11. With regard to the Brillouin data one finds several differences. Notice especially the anomaly at T_i, which is completely wiped out in our Brillouin results, probably because of fluctuations of the order parameter. In addition we observe a small anomaly which reveals the PT at $T_{L'}$. We can say globally that all the transitions are more pronounced. The behavior of $\gamma_4(\mathbf{b})$ (Fig. 10) agrees with the previously reported ones[10,11] including the hysteresis effects in the IC phase. The other presented curves, γ_3, $\gamma_5(\mathbf{c})$, $\gamma_6(\mathbf{b})$ (Fig. 12), agree with our Brillouin results. Here the transition at $T_{L'}$ is not observed; it has to be noted, however, that the damping of echoes related to $\gamma_6(\mathbf{b})$ progressively increases below T_L and that the echoes vanish just near 208 K. The attenuation of the ultrasonic waves was also measured: only very slight anomalies were found at T_i, while, for all the constants related to the phonons propagating along the **b** axis [$\gamma_2(\mathbf{b})$, $\gamma_4(\mathbf{b})$, and $\gamma_6(\mathbf{b})$] a strong attenuation was observed within a very sharp temperature interval around T_L (≈ 0.5 K), probably resulting from macroscopic displacements accompanying the corresponding first-order PT. This is illustrated in Fig. 13 as an example.

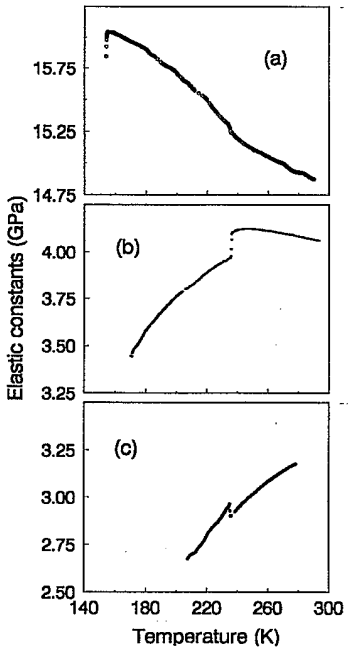

FIG. 12. Variations versus temperature of (a) γ_3, (b) $\gamma_5(\mathbf{c})$, and (c) $\gamma_6(\mathbf{b})$ measured by ultrasonic-wave propagation.

VI. CONCLUSION

The incommensurate sequence, as well as the III↔IV phase transition, induces variations in the elastic proper-

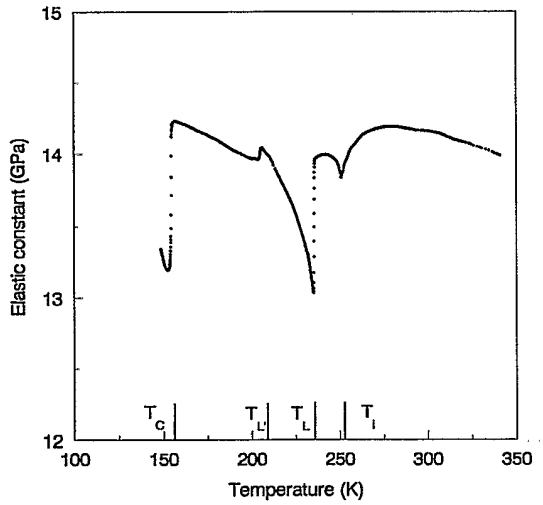

FIG. 11. Variation of γ_2 versus temperature measured by ultrasonic-wave propagation.

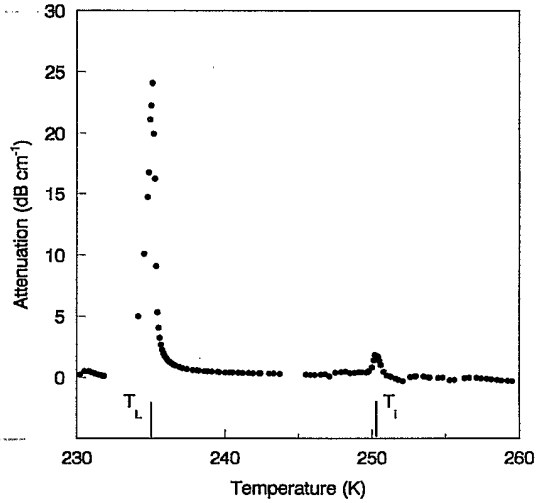

FIG. 13. Attenuation of the transverse mode related to $\gamma_4(\mathbf{b})$ measured by ultrasonic propagation.

ties of Cs_2CdBr_4 which have been experimentally studied and detected both by ultrasonic and by Brillouin-scattering measurements. Our ultrasonic investigations extend down to temperatures lower than the previously published ones and, therefore, they allow us to investigate the transition at T_C; for higher temperatures our results agree reasonably well with previous data. The previously reported attempt[8] to give an interpretation of the elastic anomalies observed by ultrasonic propagation used a static model based on a Landau development of the free energy, including appropriate couplings to strains. In view of the most probable scenario of the phase-transition mechanisms, we have justified the form of this development, after slight modifications. In the following discussions, we have examined the pertinence of such a static model in order to interpret ultrasonic and Brillouin measurements, at least qualitatively: it appears that the agreement mainly concerns some aspects of the bilinear couplings ($fQ_1\varepsilon_4, hQ_2\varepsilon_6$) or of the temperature-dependent bilinear coupling in the monoclinic phase ($gQ_1^2Q_2\varepsilon_5$), which lead to significant softenings of the transverse shear elastic constants. However, in many other respects, the agreement is poor. Brillouin and ultrasonic data markedly differ from each other, mainly concerning the elastic properties related to ε_4 in the vicinity of the I↔II phase transition around T_i; obviously, this is related to dynamic effects, which give rise to very different behaviors when studied through ultrasonic methods at a given relatively small frequency (a few tens of megahertz) and through Brillouin scattering at a given wave vector and at significantly higher frequencies (a few tens of gigahertz). In the following paper, after a detailed analysis of the predictions of the static model which was only schematically performed in the preceding sections, we shall introduce the coupled dynamics of the order parameter and of the strains, mainly in order to give account of the experimental data related to ε_4. We shall also comment on the role of fluctuations, principally in order to explain the nearly vanishing effects of the phase transition at T_i on the behavior of C_{22}.

ACKNOWLEDGMENTS

The authors thank Dr. P. Vaněk of the Institute of Physics in Prague and Dr. T. Breczewski of U.P.V. for providing them with excellent single crystals on which all Brillouin and ultrasonic measurements were performed. They also thank Dr. J. Raphanel of Laboratoire PMTM who suggested improvements for the manuscript. Finally, one of them (A.G.C) is thankful to the Spanish DGICTY for financial support.

[1]D. Altermatt, A. Niggli, W. Petter, and H. Arend, Mater. Res. Bull. **14**, 1391 (1979).
[2]S. Plesko, R. Kind, and H. Arend, Ferroelectrics **26**, 703 (1980).
[3]S. Plesko, R. Kind, and H. Arend, Phys. Status Solidi A **61**, 87 (1980).
[4]M. Maeda, A. Honda, and N. Yamada, J. Phys. Soc. Jpn. **52**, 3219 (1983).
[5]D. Altermatt, H. Arend, V. Gramlich, A. Niggli, and W. Petter, Acta Crystallogr. B **40**, 347 (1984).
[6]N. L. Speziali and G. Chapuis, Acta Crystallogr. B **45**, 20 (1988).
[7]V. Zaretskii and W. Depmeier (unpublished).
[8]V. Rodriguez, M. Couzi, A. Gomez-Cuevas, and J. P. Chaminade, Phase Transitions B **31**, 75 (1991).
[9]O. G. Vlokh, A. V. Kityk, O. M. Mokryi, B. V. Kaminskii, and V. G. Gribik, Sov. Phys. Crystallogr. **35**, 138 (1990).
[10]O. G. Vlokh, A. V. Kityk, O. M. Mokryi, and V. G. Gribik, Ukr. Fiz. Zh. **35**, 1093 (1990).
[11]O. G. Vlokh, A. V. Kityk, O. M. Mokryi, and V. G. Gribik, Sov. Phys. Solid State **33**, 181 (1991).
[12]A. P. Levanyuk and D. G. Sannikov, Sov. Phys. Solid State **18**, 1147 (1976).
[13]S. Plesko, V. Dvořák, R. Kind, and A. Treindl, Ferroelectrics **36**, 331 (1981).
[14]V. I. Torgashev, Y. I. Yuzyuk, L. A. Burmistrova, F. Smutný, and P. Vaněk, J. Phys. Condens. Matter **5**, 5761 (1993).
[15]V. Dvořák and R. Kind, Phys. Status Solidi B **107**, K 109 (1981).
[16]M. Quilichini, V. Dvořák, and P. Boutrouille, J. Phys. I (France) **1**, 1321 (1991).
[17]F. Ganot, C. Dugautier, P. Moch, and J. Nouet, J. Phys. C **15**, 801 (1982).
[18]R. Vacher and L. Boyer, Phys. Rev. B **6**, 639 (1972).
[19]D. F. Nelson and M. Lax, Phys. Rev. Lett. **24**, 379 (1970).
[20]I. L. Fabelinskii, *Molecular Scattering of Light* (Plenum, New York, 1968), p. 139.
[21]F. Ganot, R. Farhi, C. Dugautier, and P. Moch. Phys. Rev. B **40**, 273 (1989).